JOURNAL OF KUFA–PHYSICS
www.uokufa.edu.iq/journals/index.php/jkp | ISSN: 2077–5830

A Plasmonic quantum dot nanolaser: effect of "waveguide Fermi energy" on material gain

*[1,2]Jamal N. Jabir [1]Sabah. M. M. Ameen [3]Amin Habbeb Al-Khursan

[1]*Dept. of Physics, College of Science, University of Basrah, Basrah, Iraq.*
[2]*Dept. of Physics, College of Education, University of Al-Qadisiyah, Diwaniyah, Iraq.*
[3]*Nassiriya Nanotechnology Research Laboratory (NNRL), College of Science, Thi-Qar University, Nassiriya, Iraq.*

*Corresponding Author E-mail: naserjam83@yahoo.com

ARTICLE INF

Article history:
Received: 22 JUL, 2019
Accepted:08 NOV, 2019
Available Online: 12 DEC, 2019

Keywords:

Plasmonics
Quantum-well wire
dot devices
Semiconductor lasers

ABSTRACT

This work studies the gain from plasmonic quantum dot (QD) nanolaser. A metal/semiconductor/metal (MSM) structure was considered to attain plasmonic nanocavity with active region contains: QD, wetting layer (WL) and barrier layers. Band alignment between layers was used to predict their parameters. Momentum matrix element for transverse magnetic (TM) mode in QD structure was formulated. Waveguide Fermi energy was introduced and formulated, for the first time, in this work to cover the waveguide contribution (Ag metal layer) in addition to the active region. High net modal gain was obtained when the waveguide Fermi energy was taken into account which means that the increment comes from the material gain not from the confinement factor. The change in waveguide Fermi energy in the valence band explained the high gain, where the valence band QD states are fully occupied referring to an efficient hole contribution.

DOI: http://dx.doi.org/10.31257/2018/JKP/2019/110213

نانوليزر بلازمون النقطة الكمية :تأثير مستوي طاقة فيرمي للدليل الموجي على التحصيل

[١و٢]جمال ناصر جابر [١]صباح مهدي محمد أمين [٣]امين حبيب الخرسان

[١]قسم الفيزياء، كلية العلوم، جامعة البصرة، البصرة، العراق.
[٢]قسم الفيزياء، كلية التربية، جامعة القادسية، الديوانية، العراق.
[٣]مختبر الناصرية لبحوث النانو تكنولوجي، كلية العلوم، جامعة ذي قار، الناصرية، العراق

الـــخُـــلاصـــة

في هذا العمل تم دراسة التحصيل الناتج من نانو ليزر بلازمون النقطة الكمية. أخذ بنظر الاعتبار التركيب (معدن/شبه موصل/معدن) لتحقيق فجوة بلازمونية- نانوية ذات منطقة نشطة تتكون من: النقطة الكمية، الطبقة الرطبة، طبقة الحاجز. وقد استخدم طريقة محاذاة الحزم لحساب معلمات تلك الطبقات. عنصر مصفوفة العزم للنمط المغناطيسي المستعرض تم

الكلمات المفتاحية:

بلازمون
نبيطات الجدار
السلك
النقط الكمومية
ليزرات اشباه الموصلات

صياغته بطريقة تلائم انتقالات النقطة الكمية. لأول مرة تم تقديم واشتقاق طاقة فيرمي لدليل الموجة، وذلك لظهور تأثير طبقة المعدن(الفضة) على خصائص التركيب. تم الحصول على اعلى صافي تحصيل عندما طاقة فيرمي لدليل الموجة تؤخذ بنظر الاعتبار في الحسابات وهذا يعني ان التحصيل العالي ليس من معامل الحصر. حيث ان التغير في طاقة فيرمي للدليل في حزمة التكافؤ للنقطة الكمية يوضح بشكل كبير التحصيل العالي.

1. INTRODUCTION

While the quantized (nano sized) active region was attained by the quantum structures: quantum wells, quantum wires and quantum dots (QDs). The work to reduce the waveguide or cavity to a nanoscale was challenged more difficulties. In the conventional semiconductor laser with nano-active region, a considerable part of the mode profile spread out into the dielectric cladding. This increases the scattering loss and then reduces gain [1]. Cladding the structure with metal reduces the field penetration. Then, the structure becomes efficient in confining the mode in a very small size. The volume of the optical mode turns below the diffraction limit with the aid of the surface-plasmon resonance [2] [3]. This is due to negative real part of permittivity at optical frequencies. Therefore, metal-semiconductor-metal (MSM) waveguide was the base of plasmonic waveguide nanocavity that supports surface-plasmon-polaritons (SPPs), however the main challenge is the significant loss of metal which require high gain active medium to balance losses [1] [4] [5]. When electromagnetic (EM) waves are propagates in metal produced surface plasmons (SPs). SPs are depending on the plasma frequency of the metal. In another case, when it is propagate into a dielectric produced a surface plasmon-polaritons (SPPs). SPPs are EM waves that propagate along the metal-dielectric interface [6]. The gain of the propagating mode in all the laser structure is the net modal gain, while the material gain is the active region gain which is a material property. The confinement factor (CF) can be defined as the power in the active material to the power of the entire wave i.e. it is the ratio of the material gain to the net modal gain. In a strong guiding structures (such as MSM), there is a high difference between refractive indices of the active and cladding layers. Moreover, the power CF definition falls in these structures [6] while the energy CF gives the physical sense in plasmonic nanolasers [7]. Due to their high gain, QD nanostructures can offer the possibility to balance high losses to metal cladding in nanolasers. In addition, QD active region can be introduced into a nanolaser as a high material gain layer. Since QD possess discrete energy states resemble those in natural atoms or molecules, QDs regarded as a zero-dimensional structure where the electronic motion is confined in all the three spatial dimensions. They exhibit unexpected characteristics due to their incredible small size with quantum mechanical behavior [5]. QD structure contains a QD layer grown into wetting layer (WL) which is in the form of a quantum well layer. These two layers (QD and WL) are covered by the barrier (B) which is in the form of bulk layer. The Fermi energy in the conventional QD structure was introduced as the global Fermi energy as it was proposed by Kim et al., where it covers the contributions of QD-wetting layer-barrier (QD-WL-B) layers [8]. Li and Ning were predicts a high net modal gain in plasmonic nanolaser (with bulk active region) and they assigned it to the slowdown in the average energy that was propagated in the structure [6] [9]. The present work models QD nanolaser where structure studied was MSM Fabry-Perot plasmonic nanocavity with QD semiconductor active region. This type of lasers can be fabricated by many methods such as

metal coating [2]. Effect of QD, WL, B and metal (M) layers was considered. Band alignment between these layers was regarded to predict their parameters. Momentum matrix element for transverse magnetic (TM) mode in the QD structure was formulated. Contribution of metal to the Fermi energy of QD nanolaser was derived. This was done through the introduction of "waveguide Fermi energy". It was included QD-WL-B-M structure contributions. The modal gain result was coincided with that of Li and Ning [6] [9]. The obtained results show that covering the structure by a metal (Ag) increases the gain by a huge value compared with that obtained from conventional QD laser. This increment on net gain came from the material gain not from the confinement factor. The material gain was increased as a result of rearrangement of Fermi energy by addition of metal which makes a pinning of the Fermi energy and then increment in material- and modal-gain. The results clarify that WL in QD-WL-B-M works as a reservoir for valance band (VB) QD states and they are fully occupied which refers to an efficient hole contribution. This gives higher gain in these structures. The obtained results were assessed with many works about metal-semiconductor contacts [10] [11].

2. SYMMETRIC SLAB WAVEGUIDE

Figure 1 shows the structure of a three-layer symmetric slab waveguide. The core region of the guide, which is called the film, has a refractive index (n_f). Another two layers are the substrate and clad which are assumed same ($n_s = n_c$). According to the geometry, there is no variation in material 'or field' along y-direction i.e. ($\frac{\partial}{\partial y} = \frac{\partial^2}{\partial y^2} = 0$) and it is assumed here that y-dimension is longer than other dimensions. In this slab waveguide, there are a finite number of guided modes and an infinite number of unguided modes propagated on it. For guided modes, it is a requisite that n_f be larger than n_s and the guided modes, which are propagated through waveguide, are either even or odd in their field distributions. Its number in the waveguide was depends on waveguide thickness d wavelength λ and refractive indices of layers (n_f, n_s).

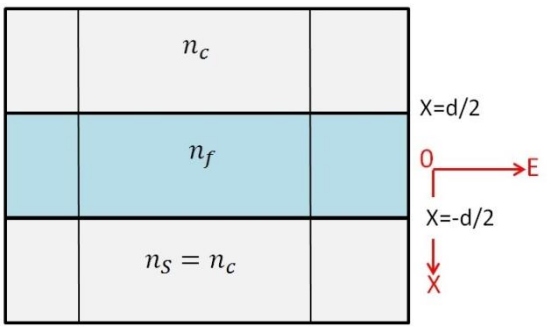

Fig. 1: Longitudinal Cross-Section of Symmetric Slab Waveguide.

Starting with Maxwell's equations, taking into account the spatial variation in the z-direction, the fields have ($e^{-ik_z z}$), and ($\frac{\partial}{\partial z} \equiv ik_z z$) dependencies.

One can define as the complex propagation constant, and as the free space propagation constant ($k = \omega\sqrt{\mu\varepsilon}$).The relation between them can be written as follows;

$$k^2 = k_x^2 + k_y^2 + k_z^2 \Rightarrow$$
$$k^2 - k_z^2 \equiv k_x^2 + k_y^2 = k_t^2 \qquad (1)$$

Where k_t is a transverse propagation constant. Critical propagation constant is given by ($k^2 - k_z^2 \equiv k_c^2$). There are several kinds of modes that can propagate through the waveguide such as: transverse electric (TE) transverse magnetic (TM) and transverse electric-magnetic (TEM) modes depending on the longitudinal components (E_z, H_z) [12].

Now, this work concentrated on two cases (TE and TM modes) in general symmetric slab waveguide but later it's consider only TM-even and -odd modes in the nanoplasmonic slab waveguide case. For TM modes which have, $E_z \neq 0,\ H_z = 0$, the transvers components of the field (E_x, E_y, H_x, H_y) are obtained as follows;

$$E_{x,y} = \mp \frac{i}{k_c^2}\{k_z \partial_{x,y} E_z\} \qquad (2)$$

$$H_{x,y} = \mp \frac{i}{k_c^2}\{\omega\varepsilon \partial_{y,x} E_z\} \qquad (3)$$

The electric field propagation in the z-direction is zero in the case of TE mode, therefore one can derive the non-zero components of the fields in symmetric slab waveguide with, $H_y = 0$, and $E_x = 0$.

$$H_x = \frac{i}{k_c^2}(k_z \partial_x H_z) \qquad (4)$$

$$E_y = -\frac{i}{k_c^2}(\omega\mu \partial_x H_z) \qquad (5)$$

Furthermore, the non-zero tangential component of the electric field is (E_y). On the other side, for TM mode, take into account $H_z = 0$, to get

$$H_y = \frac{i}{k_c^2}(\omega\varepsilon \frac{\partial E_z}{\partial x}) \qquad (6)$$

$$E_x = -\frac{i}{k_c^2}(k_z \frac{\partial E_z}{\partial x}) \qquad (7)$$

With $H_x = 0$ and $E_y = 0$. Then, the non-zero tangential component of the magnetic field is, H_y. One can write, E_x using, H_y as following;

$$E_x = -\frac{k_z}{\omega\varepsilon} H_y \qquad (8)$$

3. THE WAVE EQUATION FOR SYMMETRIC SLAB WAVEGUIDE

Consider a symmetry slab waveguide is shown in Figure 2 with Ag-metal as cladding and QD-WL-B (from InAs-InGaAs-GaAs, respectively) as core region. Maxwell's equations can be written in terms of the permittivity of materials ($\varepsilon_i, i = f, s$), of the layers, assuming that the material of each one is non-magnetic and isotropic, i.e. $\mu_i = \mu_o$. For TE modes, $E_z = 0$ and the non-zero component of the electric field is E_y, while for TM modes, $H_z = 0$ and the non-zero component of the magnetic field was H_y. Therefore, the wave equation for two cases, after noting $\frac{\partial^2}{\partial y^2} = 0$ and $\frac{\partial}{\partial z} = ik_z z$, can be written as,

$$(\frac{\partial^2}{\partial x^2} + k_c^2)\begin{Bmatrix} E_y \\ H_y \end{Bmatrix} = 0 \qquad (9)$$

$$k_c^2 = (\omega^2 \mu_o \varepsilon_i - k_z) \Rightarrow$$
$$k^2 - k_z^2 = k_o^2 n_i^2 - k_z^2 \qquad (10)$$

Where ε_i and n_i are the relative permittivity and refractive index at each layer ($i = f, s$). Since this work specialized waveguide that both cladding and substrate are metal, the film is dielectric i.e. plasmonic slab waveguide. One must deal with TM modes only which are the most confined at the interface of core-metal [13] [14]. The electric field in the core region have an even function; $\cos(k_x), \cosh(k_x)$, and an odd function; $\sin(k_x), \sinh(k_x)$, that is depending on the wavelength. Also, electric field was decay exponentially in the cladding or substrate [15] [16]. Now, the magnetic field for

an even and odd mode can be written, respectively, in the form;

$$H_y(x)=e^{ik_z z}\begin{cases}c_o e^{-\alpha(x-d/2)} & at \quad x \geq d/2\\ c_1\cosh(k_x x) & at \quad |x| \leq d/2\\ c_o e^{\alpha(x+d/2)} & at \quad x \leq -d/2\end{cases} \quad (11)$$

$$H_y(x)=e^{ik_z z}\begin{cases}c_o e^{-\alpha(x-d/2)} & at \quad x \geq d/2\\ c_1\sinh(k_x x) & at \quad |x| \leq d/2\\ c_o e^{\alpha(x+d/2)} & at \quad x \leq -d/2\end{cases} \quad (12)$$

By substituted Eqs. (11) and (12) into Eq.(9) one can obtain the following relations inside and outside the guide;

$$k_x^2+k_z^2=\omega^2\mu_1\varepsilon_1 \ \ (inside) \quad (13)$$

$$-\alpha^2+k_z^2=\omega^2\mu\varepsilon \ \ (outside) \quad (14)$$

Where the dielectric constant of semiconductor is (ε_1), and (ε) is dielectric constant of metal. From Maxwell's equations one can derive TM mode component of $E_z(x)$. Notes that $H_y(x)=\hat{y}H_y$, ($H_x=H_z=0$), and ($E_z\neq 0, E_x\neq 0, E_y=0$. So, one becomes able to write H_y by E_x and one has ($\partial_x^2 E_z=-k_c^2 E_z$). Then, the wave equation becomes;

$$E_z=\frac{i}{\omega\varepsilon}\frac{\partial H_y}{\partial x} \quad (15)$$

The graphical solution was used to find the propagation constant k_z after obtaining the eigen-equations by matching the boundary conditions in H_y (Eqs. 11 and 12) and E_z which are continuous at, $x=\pm d/2$. From equations 13 and 14, k_z must eliminated. The graphical solution [17] [18] give us α and k_x .To obtain the normalization constants (c_o, c_1) for the optical mode first, the power P_z flows along z-direction in the film layer is given by [12];

$$P_z(x)=\frac{1}{2}\mathrm{Re}\{\int_{-\infty}^{+\infty}(E\times H^*).\hat{z}\,dx\}=1 \quad (16)$$

$$P_z(x)=\frac{1}{2}\frac{\omega\varepsilon}{k_z}\int_{-\infty}^{+\infty}|E_x(x)|^2\,dx=\frac{1}{2}\frac{k_z}{\omega\varepsilon}\int_{-\infty}^{+\infty}|H_y(x)|^2 dx \quad (17)$$

$$c_1=\sqrt{\frac{4\omega^2\varepsilon^2}{k_z^2(k_x d+\sinh(k_x d))}} \quad (18)$$

$$c_o=c_1\cosh(k_x d) \quad (19)$$

4. OPTICAL CONFINEMENT FACTOR

In this section, let's going to derive the optical confinement factor in general formula and later it's specialized to plasmonic nanocavity waveguide. The optical confinement factor is defined as the ratio of the squared electric field that is restricted in the active region. Derivation of the optical confinement factor can be found from Maxwell's equations for TM modes, following a procedure similar to [16]. Using field components, the power confinement factor can be written as;

$$\Gamma_p=\frac{P_z}{P_T}=\frac{\int_{A_a}\mathrm{Re}[\frac{1}{2}E_x(x)\times H_y^*(x)]dxdy}{\int_{A}\mathrm{Re}[\frac{1}{2}E_x(x)\times H_y^*(x)]dxdy} \quad (20)$$

Where, A_a is the cross-section of the active region, and A is the area of the plasmonic waveguide. Non-zero components that are working in the waveguide are E_x , and H_y. Another type of optical confinement factor is called energy confinement factor (Γ_E), which have values that must be less than unity (i.e. $\Gamma_E<1$) because an optical modes cannot overlap perfectly with the active region [7]. This condition holds in plasmonic cavities in which the real part of the metal permittivity is negative [19]. The energy confinement factor is given by،

$$\Gamma_E=\Gamma_z\,\Gamma_{E,t} \quad (21)$$

Where $\Gamma_{E,t}$ is the transverse energy confinement factor, which is written in terms of nonzero component of TM modes as, E_x;

$$\Gamma_{E,t} = \frac{\int_{A_a} \frac{\varepsilon_o}{4}\varepsilon_a |E_x(x)|^2 dx}{\int_A \frac{\varepsilon_o}{4}\varepsilon_a |E_x(x)|^2 dx} \quad (22)$$

While Γ_z is a longitudinal confinement factor. For its derivation, suppose that the waveguide as in Fig. 1 (c). In the active region, assuming the solutions are of the form;

$$U_a(z) = \begin{cases} A\cosh(k_z z) \rightarrow (\text{even solutions}) \\ A\sinh(k_z z) \rightarrow (\text{odd solutions}) \end{cases} \quad (23)$$

Where U_a is the field in the active region, depend on x-direction. The propagation constant is $k_z = \sqrt{k_o^2 n_a^2 - k_x^2}$, with k_o, n_a and k_z are the propagation constant in free space, refractive index of the active region, and the complex propagation constant, respectively, as in previous section. The longitudinal confinement factor Γ_z, can be defined as;

$$\Gamma_z = \frac{1}{L}\left(\int_{-d/2}^{+d/2} |U_a(z)|^2 dz\right) \quad (24)$$

Where L and d are the length and thickness of the active region, respectively. For even and odd modes, one can be obtained;

$$\Gamma_z = \frac{d}{L_a}\sqrt{\frac{1}{d/2 + \sinh(k_z d/2)}}\left(1 + \frac{\sinh(k_z d)}{(k_z d)}\right) \quad (25)$$

$$\Gamma_z = \frac{d}{L_a}\sqrt{\frac{1}{d/2 + \cosh(k_z d/2)}}\left(1 + \frac{\cosh(k_z d)}{(k_z d)}\right) \quad (26)$$

The transverse confinement factor is given by [18];

$$\Gamma_{xy} = \frac{\int_{-w/2}^{+w/2}\int_{-d/2}^{+d/2} |U_a(x,y)|^2 dx\, dy}{\iint_{xy} |U_a(x,y)|^2 dx\, dy} \quad (27)$$

5. MATERIAL GAIN OF PLASMONIC QD NANOLASER

The material gain of QDs plasmonic nanostructure depends on the Fermi distributions f_c, f_v into conduction (CB) and valence bands (VB), respectively. MSM plasmonic QDs nanocavity composed from Ag metal cladding-substrate layers, and active region composed from: GaAs (B), InGaAs (WL) and InAs (QD), Fig. 2 (c). QDs were assumed to be in the form of quantum disks. Using a disk radius of a=14 nm and a height of h=2 nm, energy subbands in the QD (InAs) and WL (InGaAs) are calculated using the quantum disk model [20].

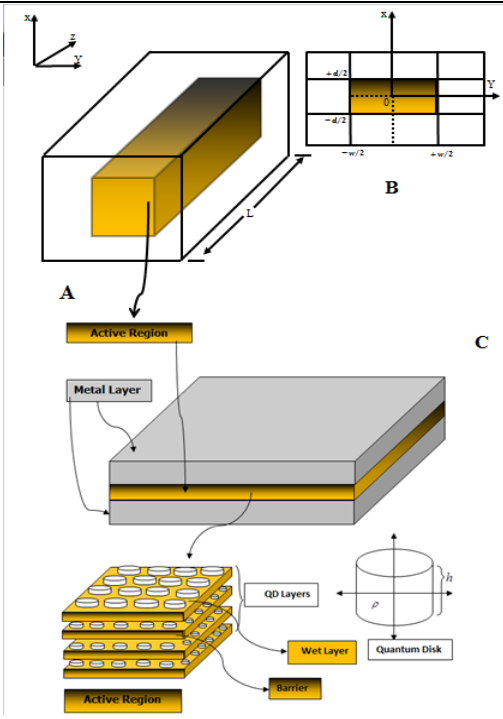

Fig. 2: General plasmonic nanolaser cavity with (L) length. (A) Longitudinal. (B) transvers cross-section. Active region has dimensions (d) in x-direction and (w) in y-direction. (C) Active region of plasmonic QD nanolaser structure.

This model was checked with experiment [5] [21]. Fig. 3 displays the calculated energy band diagram of plasmonic QDs nanostructure. For MSM band alignment, the band-edge discontinuity of Ag/GaAs i.e. M/B was

calculated in CB as, $\Delta E_c^{(M/B)} = E_c^M - E_c^B$, taking $E_c^M \equiv Q_m$, with Q_m is the work function of Ag metal. For B/QD, $\Delta E_c^{B/QD} = E_c^B - E_c^{QD} = Q_c \Delta E_g$, and $\Delta E_g = E_g^B - E_g^{QD}$. Note that, E_c^i and E_v^i represents CB and VB edges, respectively, with the superscript i refers to either of M, B, WL, QDs layer. QDs and WL materials are not much different, so taking the difference between GaAs/InAs to calculate their band edge discontinuity.

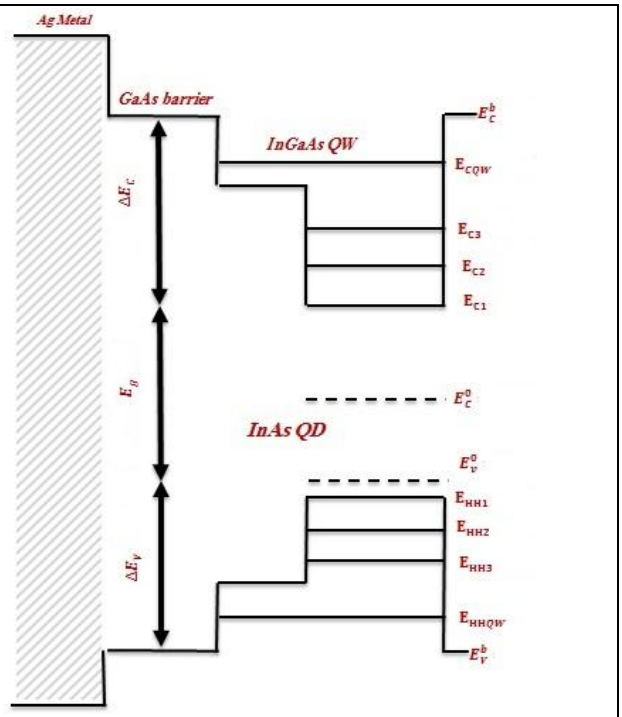

Fig. 3. Band Energy diagram of the plasmonic QDs nanolaser structure.

The band-edges in VB were calculated by the same way using $Q_v = 1 - Q_c$. Note that Q_c and Q_v are the partition ratios of the band edge discontinuities. Since both E_c^B and E_c^{QD} are obtained, $\Delta E_c^{(M/B)}$ can be obtained. The optical transitions are occur between (e1-hh1), (e2-hh2) and (e3-hh3), respectively where (e_i-hh_i) with the subscript (i=1, 2 and 3) refers to the ith conduction electron-heavy hole transitions. The material gain is calculated from the relation [20];

$$g(\hbar\omega) = \frac{\pi e^2}{n_B c \varepsilon_o m_o \omega} \sum_i \int_{-\infty}^{+\infty} dE' \left|M_{env}\right|^2 \left|\hat{e}.p_{cv}\right|^2 \times D(E') L_g(E', h\omega)[f_c(E', F_c) - f_v(E', F_v)] \quad (28)$$

The summation runs overall the radiative transitions. The terms ω, n_b, c, ε_o, m_o, E' and M_{env} are the angular optical frequency, the background refractive index of the material, the speed of light in free space, the permittivity of free space, the free electron mass, the optical transition energy, and the envelope function overlap between the QD electron and hole states, respectively. It is assumed that the envelope function overlap is nearly an unity between the QD electron and hole states of the same quantum numbers [20]. The term $D(E')$ represents the inhomogeneous broadening of QDs, which is the density of states of self-assembled QDs, and σ the spectral variance of QDs.

In Eq. (28), the term $|\hat{e}.p_{cv}|$ is the momentum matrix of QDs and it depends on the polarization of the light. Because of this work dealing with metal-coated structure, only the momentum matrix element for TM polarization in the case $e-hh$ of transition was taken. The momentum matrix element of plasmonic QDs is developed from [17] as the following relation;

$$\left\langle \left|\hat{e}.p_{e\text{-}hh}\right|^2 \right\rangle = \frac{3}{2}(1-\cos^2\theta)M_b^2 = \frac{3}{2}\left(1-\frac{E_{cym}}{E_{cnml}}\right)M_b^2 \quad (29)$$

Where, $M_b^2 = \left(\frac{m_o}{6}\right)E_p$, and E_p is optical matrix energy parameter.

6. WAVEGUIDE FERMI ENERGY

In order to calculate the net modal gain for plasmonic nanostructure, band parameters must be set. Thus, the band alignment for InAs (QD)/InGaAs (WL)/GaAs (barrier)/Ag (metal) layers was done as stated above. Since the optical gain of the plasmonic QD nanolaser was investigated in this study at room temperature,

the carrier distribution can be assumed to be in quasi-equilibrium. For the QD nanolaser structure under study, one can determine quasi-Fermi levels in the CB (F_c) and VB (F_v) numerically from the surface carrier density per QD layer as following,

$$n_{2D}=N_D\sum_i \frac{s^i}{\sqrt{2\pi\sigma_e^2}}\int e^{-(E_c^{'}-E_{ci}^{D})^2/2\sigma_e^2}\frac{1}{1+e^{(E_c^{'}-F_c)/K_BT}}dE_c^{'}$$
$$+\sum_l\sqrt{\frac{m_e^w k_B T}{\pi h}}\ln(1+e^{(F_c-E_{el}^w)/k_BT})$$
$$+t_B\int\frac{1}{2\pi^2}\left(\frac{2m_e^B}{h^2}\right)^{3/2}\sqrt{E_c^{'}-E_c^B}\frac{1}{1+e^{(E_c^{'}-F_c)/K_BT}}dE_c^{'}$$
$$+t_M\int\frac{1}{2\pi^2}\left(\frac{2m_e^M}{h^2}\right)^{3/2}\sqrt{E_c^{'}-E_c^M}\frac{1}{1+e^{(E_c^{'}-F_c)/K_BT}}dE_c^{'} \quad (30)$$

$$p_{2D}=n_{2D}=N_D\sum_j \frac{s^j}{\sqrt{2\pi\sigma_h^2}}\int e^{-(E_h^{'}-E_{hj}^{D})^2/2\sigma_h^2}\frac{1}{1+e^{(F_v-E_h^{'})/k_BT}}dE_h^{'}$$
$$+\sum_m\frac{m_h^w k_B T}{\pi h}\ln(1+e^{(F_v-E_{hm}^w)/k_BT})$$
$$+t_B\int\frac{1}{2\pi^2}\left(\frac{2m_h^B}{h^2}\right)^{3/2}\sqrt{(E_h^B-E_h^{'})}\frac{1}{1+e^{(F_v-E_h^{'})/k_BT}}dE_h^{'}$$
$$+t_M\int\frac{1}{2\pi^2}\left(\frac{2m_h^M}{h^2}\right)^{3/2}\sqrt{(E_h^M-E_h^{'})}\frac{1}{1+e^{(F_v-E_h^{'})/k_BT}}dE_h^{'} \quad (31)$$

The electrons and holes surface densities per QD layer are n_{2D} and p_{2D}, respectively. E_{ci}^D and σ_e are i^{th} maximum and the spectral variance of the QD electron distribution, respectively. In the same manner, E_{hj}^D and σ_h are the j^{th} maximum and the spectral variance of the QD heavy-hole distribution. The terms $E_c^{'}$ ($E_h^{'}$), $m_e^w\,(m_h^w)$, $E_{el}^w\,(E_{hm}^w)$, t_B, $m_e^B\,(m_h^B)$, $E_c^B\,(E_h^B)$, t_M, $m_e^M\,(m_h^M)$, $E_c^M\,(E_h^M)$ are the QD subband energy in the CB (VB), the effective electron (hole) mass, the subband edge of the CB (VB) of the InGaAs wetting layer (WL), the thickness of the GaAs barrier layer, the carrier masses, the band edge of the CB (VB) of the GaAs barrier layer, the thickness of the Ag metal layer, the carrier mass and the band edge of the CB (VB) of the Ag metal layer, respectively. Relations of conventional QD laser that covers B, WL, and QD contributions are only discussed in [17] [8]. In this work, Eqs. (30) and (31) are covering the metal contribution to QD nanolaser gain. In this work it's suitable calling F_c and F_v in these relations as "waveguide Fermi energies". In other side the modal gain g_M can be defined by relation [23]; as follow;

$$g_M(\hbar\omega)=\Gamma_{xy}\,g(\hbar\omega) \quad (32)$$

Where g_M, Γ_{xy} and $g(\hbar\omega)$ are modal gain, optical confinement factor, and material gain, respectively.

7. RESULTS AND DISCUSSIONS

Figures 4 (a) and (b) shows TM modes of where an even and odd function behavior was seen.

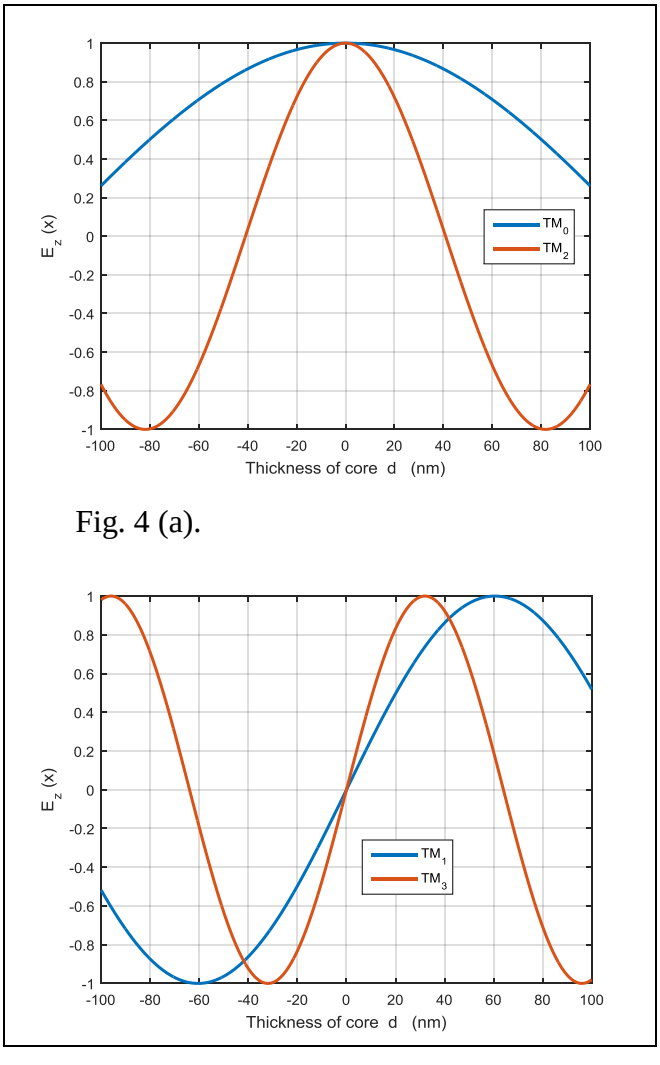

Fig. 4 (a).

Fig.4 (b).

Fig. 4: Electric field profiles, versus core thickness for: (a) even modes (b) odd modes, in QD semiconductor active region.

Figure 5(a) shows the energy confinement factor (ECF) in the transverse direction ($\Gamma_{E,t}$), where the confinement was reduced with energy. The energy confinement factors for even and odd modes will diverge with transition energy. This behavior was contradicted to the confinement factor along z-axis, Γ_z, in Fig. 5 (b). Fig. 5 (c) illustrated the total ECF where it was increased with photon energy spectrum. The even and odd curves of total ECF are separated at high energy.

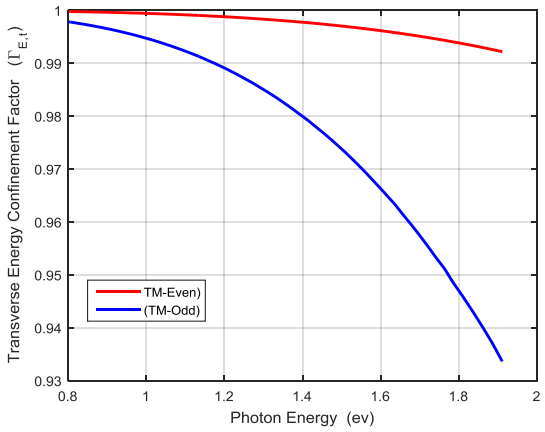

Fig. 5 (a).

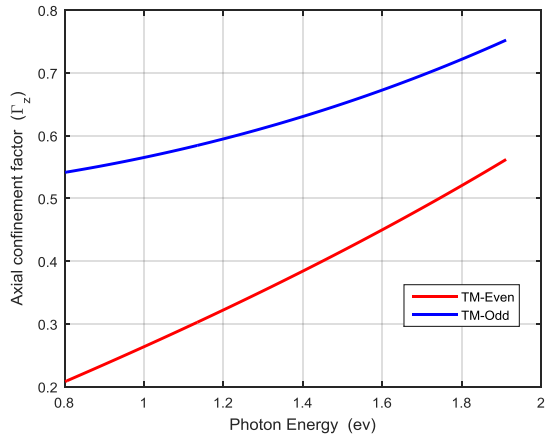

Fig. 5 (b).

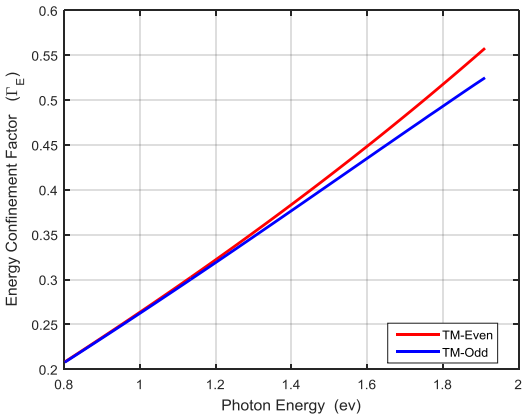

Fig.5 (c).

Fig. 5: (a) Transverse, (b) axial, and (c) total Energy confinement factor versus photon energy.

Fig. 6 (a and b) shows the optical confinement factor in the transvers direction (Γ_{xy}) where it was very low (three orders) comparing with ECF.

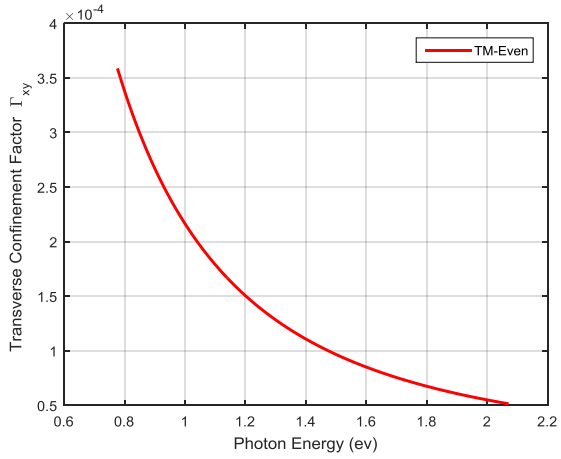

Fig. 6 (a).

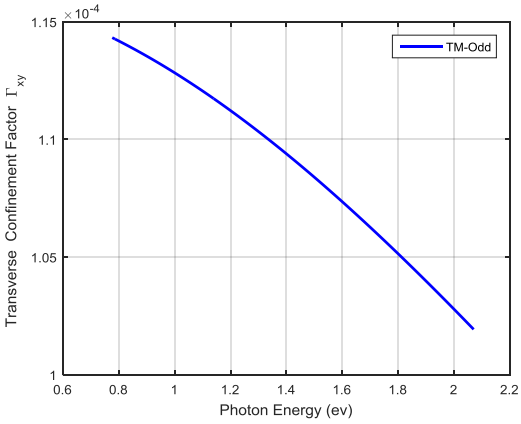

Fig. 6 (b).

Fig. 6: The optical confinement factor for (a) even and (b) odd modes versus photon energy.

Fig. 7 indicates the power confinement factor (PCF) for the even and odd modes have values higher than unity due to the metal contribution.

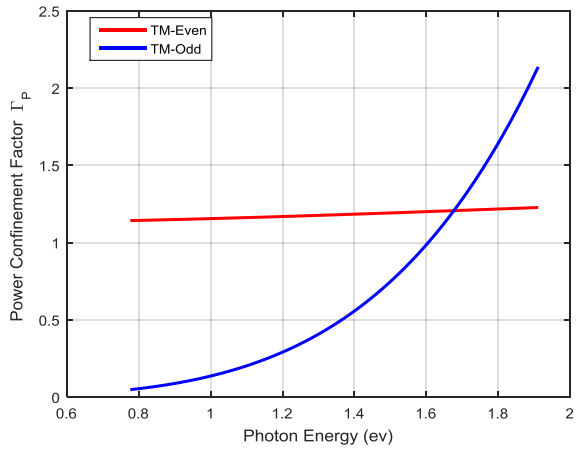

Fig. 7: The power confinement factor for even mode (red), and odd mode (blue line) versus photon energy.

One can see in Fig. 8 the net modal gain for conventional QD structure (QD-WL-B). The peak net modal gain of QD-WL-B was $100cm^{-1}$ which is in the range of Kim and Chuang results [20].

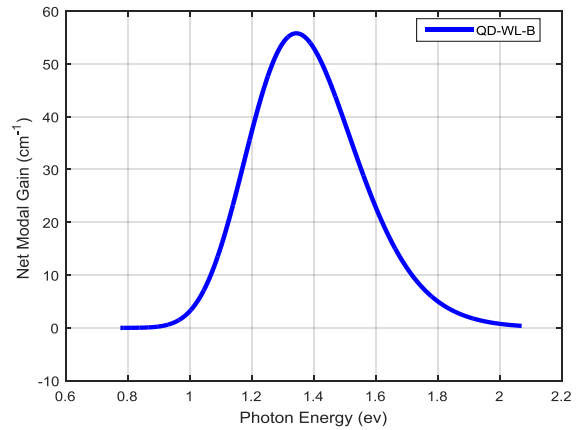

Fig. 8: Net modal gain of QD-WL-B (blue curve), structures are plotted versus photon energy.

Fig. 9 clarifies the net modal gain for plasmonic QD nanolaser structure (QD-WL-B-M). Note that the value of QD-WL-M gain was in the range of [7] who also deals with the MSM structure (but with bulk active region). Note that the value of gain obtained here overcomes the electron scattering losses (10^{15} fs) [24].

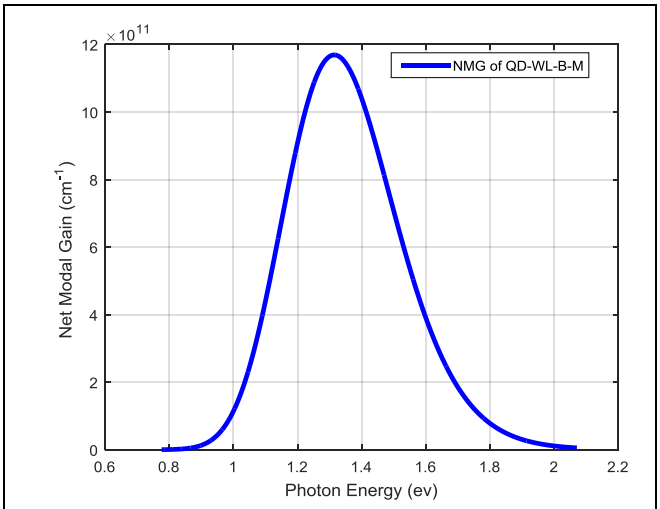

Fig. 9: Net modal gain of QD-WL-B-M (blue curve), structures are plotted versus photon energy.

To see the reason for this high gain, the Fermi energies in the conduction (Fc) and valence (Fv) bands were plotted versus surface carrier density for conventional plasmonic QD nanolaser. The figure also show the main difference that this work differs from others [6] [9] which deals with plasmonic structures. In [6] [9] Li and Ning ascribe the high modal gain to the slow-down of the average energy that propagates in the structure which gives a high confinement factor. In the present study, metal contribution was included in the Fermi energy calculations of QD nanolaser. Already only the active region was considered for Fermi energy calculations in conventional QD laser, for example see [8] [20]. Addition of metal was rearranged the Fermi energy as discussed by the literature discussing MSM structures [10] [11]. For the first time, our team added Fermi energy

that covers metal contribution and that is calling in this work as; “waveguide Fermi energy”.

Figure 10 shows Fermi energy in CB, , for the two structures studied. For the conventional QD laser i.e. QD-WL-B structure, a high was obtained. Covering the structure by a metal (Ag) which is the case of QD plasmonic nanolaser structure i.e. QD-WL-B-M, the waveguide Fermi energy curve was same as the first case of conventional laser (QD-WL-B).

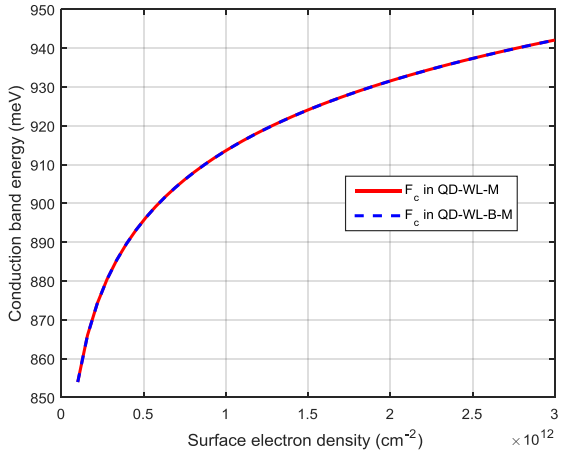

Fig. 10: CB quasi Fermi levels in (QD-WL-B) structures.

Figure 11 plots the Fermi energy in VB, F_v , of conventional QD (QD-WL-B) structure as in blue curve compared with that of plasmonic QD nanolaser structure (QD-WL-B-M) as in maroon curve. F_v in conventional, QD-WL-B, structure was shown near the top of VB. After adding the metal (QD-WL-B-M structure) i.e. the waveguide Fermi energy of plasmonic QD nanolaser structure, F_v goes down deeper than F_v into conventional structure by approximately 72meV. So the main change in F_v comes from adding metal. This may be attributed to the work function of metal which makes Fermi level de-pinning.

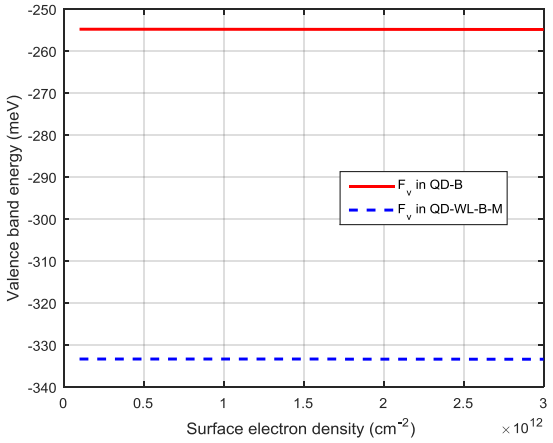

Fig.11: VB quasi Fermi levels difference in (QD-WL-B-M) structures.

From Figs. 10 and 11, the smallest F_c for QD-WL-B in Fig. 10 was 855meV at carrier density, while the highest Fc was 942meV at, $3\times10^{12}cm^{-2}$. Fv=-255meV for QD-WL-B and -332meV for QD-WL-B-M. So, the smallest transparency points (Fc-Fv) in conventional and plasmonic structures were 1110 meV, 1187 meV, respectively, while their highest transparency points were 1197, 1274meV i.e. the difference between the smallest and highest transparency points was 87meV. In plasmonic structure, the transparency point becomes wider by 77meV than conventional one. This means that covering the structure with metal was permitted most of the active region transitions to contribute as in beneficial transitions. This was in the contrary to the conventional QD laser structures, where not all of them were contributed since some of them were below the transparency. In another words, in Figs. 10 and 11, F_v in QD-WL-B-M structure goes deeper in VB than conventional QD-WL-B structure. Thus, for Fermi levels in metallic guiding structures de-pinning F_v in VB means that the transparency energy ($Fc-Fv$) lies near the VB edge of GaAs barrier. So, WL in QD-WL-B-M works as a reservoir for VB QD states and they are fully occupied which refers to an efficient hole contribution. This gives higher gain in these structures. Conventional QD structures

suffer from weak hole contribution (which requires p-doping) [8].

The results obtained here were coinciding with the conclusion of [25]. They find experimentally that when metal/semiconductor contact resistivity was reduced the performance was improved. Schottky barrier heights ($q\phi_m$) must be reduced to get a low resistivity. Pinning Fermi-level close to VB in this work stiffs the low ($q\phi_m$)[25]. Because of the optical confinement factor is changed by adding metal as coming along with the results of Chuang and Chang in [7]. It is not explains the net gain increment, see Fig. 6. So that, plotting the material gain for these two structures in Figs. 12 and 13. For QD-WL-B, Fig. 12 simulates the results that are obtained by conventional QD laser and its values are in the range of that in [8] [20].

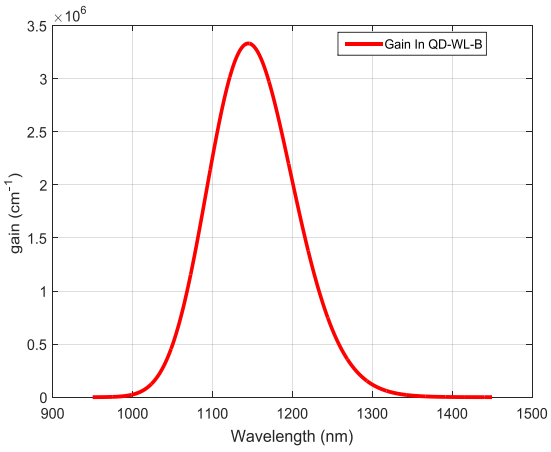

Fig. 12. Material gain for conventional QD laser (QD-WL-B) structure.

For QD-WL-B-M, Fig.13 gives result that not justifiyed by conventional QD laser. Returning to Figs. 10 and 11, they are obviously showing the effect of cladding the structure by metal. The metal was rearranged the Fermi energy, pinning it to a higher value, and then changing the material gain dramatically.

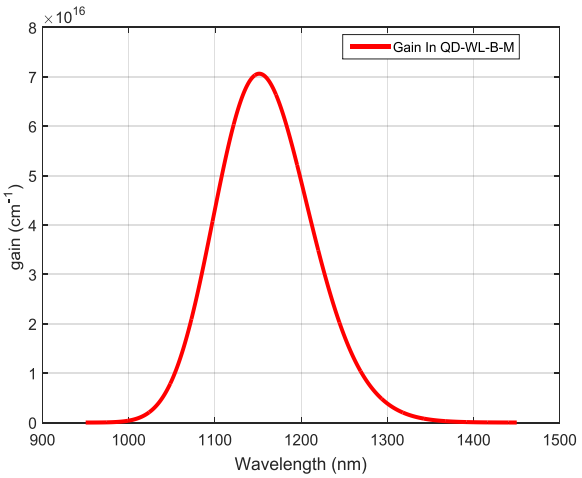

Fig.13. Material gain spectra for plasmonic QD nanolaser with QD-WL-B-M structure.

8. CONCLUSIONS

This work deals with modal gain in plasmonic QD nanolaser. TM modal gain and waveguide confinement factor were modeled. Metal contribution was covered through the waveguide Fermi energy. High net modal gain was obtained when the waveguide Fermi energy was taken into account.

9. REFERENCES

[1] S. W. Chang, T. R. Lin and S. L. Chuang, "Theory of plasmonic Fabry-Perot nanolasers", Optics Express 18, 15039-15053 (2010).

[2] C. Y. Adrian Ni, S. W. Chang, D. J. Gargas, M. C. Moore, P. Yang and S. L. Chuang, "Metal-Coated Zinc Oxide Nanocavities", IEEE J. Quantum Electron. 47, 245-251 (2011).

[3] C. Y. Lu and S. L. Chuang, "A surface-emitting 3D metal-nanocavity laser: proposal and theory", Optics Express 19, 13225-13244 (2011).

[4] S. W. Chang, C. Y. Adrian Ni and S. L. Chuang, "Theory for bowtie plasmonic nanolasers", Optics Express 16, 10580-10595 (2008).

[5] S. N. Dwara and Amin H. Al-Khursan, "Quantum Efficiency of InSbBi Quantum Dot photodetector", Applied Optics 54, 9722-9727 (2015).

[6] D. B. Li and C. Z. Ning, “Peculiar features of confinement factors in a metal-semiconductor waveguide”, Appl. Phys. Lett. 96, 181109 (2010).

[7] S. W. Chang and S. L. Chuang, "Fundamental Formulation for Plasmonic Nanolaser", IEEE J. Quantum Electronics 45, 1014-1023 (2009).

[8] J. Kim, M. Laemmlin, C. Meuer, D. Bimberg and G. Eisenstein, "Static Gain Saturation Model of Quantum-Dot Semiconductor Optical Amplifiers" IEEE J. Quantum Electronics 44, 658-666 (2008).

[9] D. B. Li and C. Z. Ning, “Giant modal gain, amplified surface plasmon-polariton propagation, and slowing down of energy velocity in a metal-semiconductor-metal structure”, Phys. Rev. B 80, 153304, (2009).

[10] H. Yu, M. Schaekers, K. Barla, N. Horiguchi, N. Collaert, A. V. Y. Thean and K. De Meyer, “Contact resistivities of metal-insulator-semiconductor contacts and metal-semiconductor contacts”, Appl. Phys. Lett. 108, 171602 (2016).

[11] A. Agrawal, J. Lin, M. Barth, R. White, B. Zheng, S. Chopra, S. Gupta, K. Wang, J. Gelatos, S. E. Mohney, and S. Datta, “Fermi level depinning and contact resistivity reduction using a reduced titania interlayer in n-silicon metal-insulator-semiconductor ohmic contacts”, App. Phys. Lett. 104, 112101 (2014).

[12] S. J. Orfanidis, Electromagnetic Waves and Antennas, Rutgers University, (2014).

[13] V. Krishnamurthy and B. Klein, "Theoretical Investigation of Metal Cladding for Nanowire and Cylindrical Micropost Lasers", IEEE J. Quantum Electronics 44, 67-74 (2008).

[14] K. Ikeda, Y. Fainman, K. Alan Shore, and Hitoshi Kawaguchi, "Modified long-range surface plasmon polariton modes for laser nanoresonators", J. Appl. Phys. 110, 063106 (2011).

[15] T. Numai, Fundamentals of Semiconductor Lasers, Springer (2015).

[16] Y. Z. Huang, Z. Pan, and R.H. Wu, "Analysis of the optical confinement factor in semiconductor laser", J. Appl. Phys. 79, 3827 (1996).

[17] S. L. Chuang, Physics of Photonic Dvices, 2nd Ed. Wiley, 2009.

[18] Larry A. Coldren and Scott W. Crozine and Milan L. Masanovic, Diode Lasers and Photonic Integrated circuits, 2nd Ed., Wiley (2012).

[19] S. W. Chang and S. L. Chuang, "Normal modes for plasmonic nanolasers with dispersive and inhomogeneous media", Optics Letters 34, 91-93 (2009).

[20] J. Kim, and S. L. Chuang, "Theoretical and Experimental Study of Optical Gain, Refractive Index Change, and Linewidth Enhancement Factor of p-Doped Quantum-Dot Lasers", IEEE J. Quantum Electron. 42, 942-952 (2006).

[21] H. Al-Husseini, Amin H. Al-Khursan and S. Y. Al-Dabagh, "III-N QD Lasers", Open Nanoscience Journal 3, 1-11 (2009).

[22] M. Asada, Y. Miyamoto, and Y. Suematsu, "Gain and the threshold of three-dimensional quantum-box lasers.", IEEE J. Quantum Electron. 22, 1915-1921 (1986).

[23] P. S. Zory, Quantum Well Lasers, Elsevier (1993).

[24] M. N. Abbas, D. S. Mohammed, “Quality Factor Improvement for Nano Cavity”, International J. of Computer Applications 127, 22-25 (2015).

[25] H. Yu, M. Schaekers, T. Schram, S. Demuynck, N. Horiguchi, K. Barla, N. Collaert, A. Thean, and K. M. De Meyer, "Thermal Stability Concern of Metal-Insulator Semiconductor Contact: A Case Study of Ti/TiO2/n-Si Contact", IEEE Transactions on Electron Devices 63, 2671-2676 (2016).